All-carbon ferromagnetism derived from edge states in graphene nano-pore arrays

K. Tada[1], S. Kamikawa[1], Y. Yagi[1], J. Haruyama[1*], T. Matsui[2], H. Fukuyama[2]

[1]Faculty of Science and Engineering, Aoyama Gakuin University, 5-10-1 Fuchinobe, Sagamihara, Kanagawa 252-5258, JAPAN

[2]Department of Physics, University of Tokyo, 7-3-1 Hongo, Bunkyo-ku, Tokyo 113-8656, JAPAN

Ferromagnetism in carbon-based materials is unique as compared to conventional ferromagnets arisen from 3*d* or 4*f* electrons, because only *s* and *p* orbital electrons form it. Many theoretical works have predicted the appearance of ferromagnetism in carbon-based systems from viewpoints of edge-localized electrons[1-7]. However, few independent observations have reported the existence of ferromagnetism in controllable systems with high reproducibility, such as poor reproducibility in uncontrollable graphite-related systems[8-10]. On the other hand, the edge structures of graphene are of particular interest[11-22]. Theoretically, the so-called zigzag edge has strongly localized electrons due to the presence of flat bands near the Fermi level[1]. The localized electron spins are also strongly polarized, resulting in the emergence of ferromagnetism[3,5,13,14]. However, no study thus far has experimentally reported ferromagnetism. Here, in the present work, we fabricate honeycomb-like array of nano-sized pores on graphenes (antidot-lattice graphene) with a large ensemble of hydrogen-terminated nano-pore edges by a non-lithographic and low-damage method using nanoporous alumina templates[3]. We observe room-temperature ferromagnetism derived from the polarized electron spins at the nano-pore edges. This promises the realization of all-carbon magnets and spintronic devices based on a spin Hall effect[22,24-27].

Ferromagnetism in graphite-related systems has been poorly demonstrated such as in highly oriented pyrolytic graphite (HOPG) detected specifically at defects[8] and activated carbon fibers (ACFs)[9]. The origin of ferromagnetism has been interpreted in terms of high electronic density of states (EDOSs, i.e., edge states), which exists at the zigzag edges of a two-dimensional (2D) array of point defects at HOPG grain boundaries and the 3D disordered network of nano-graphite domains in ACFs. However, the origin of ferromagnetism remains ambiguous because of those complicated and uncontrolled structures. Only edge states have been possibly observed in graphite using scanning tunnel microscopy (STM)[10].

On the other hand, the zigzag edge of graphene has theoretically high EDOSs owing to its strongly localized electrons (edge states), which have been introduced by presence of flat bands near the Fermi level (E_F)[1]. The localized electron spins are strongly polarized depending on the spin interaction between two edge lines (e.g., in graphene nanoribbons (GNRs) that are 1D restriction of graphene with edges on both longitudinal sides) and become responsible for magnetic behaviour such as ferromagnetism or antiferromagnetism[3,5-7,13,14]. This is because the nonbonding states of carbon atoms (i.e., dangling bonds) at the zigzag edge are half filled and behave like the outer shell of a ferromagnetic atom, which is not stable when spin is taken into account. The exchange interaction requires the spin in these orbitals to be maximized, similar to Hund's rule for atoms. It determines whether either ferromagnetism or antiferromagnetism appears in GNRs, which in turn strongly depends on the termination of edge carbon atoms by foreign atoms (e.g., hydrogen or oxygen).

Many works have theoretically predicted the appearance of ferromagnetism in graphene-related systems such as GNRs[1-7], antidot-lattice graphenes (ADLGs) with honeycomb-shaped antidots[13], and graphene nano-flakes (nano-islands) with triangular and hexagonal shapes[14]. However, there have been no reports of the experimental observation of ferromagnetism, although experiments to observe and control graphene edge structures have been conducted using approaches such as Joule heating with an STM probe[15], fabrication of GNRs[17-19], and formation of ADLGs with edges around the antidots[20,21].

Figure 1a shows the top view of a scanning electron microscopy (SEM) image of a nanoporous alumina template[23] (Al_2O_3; NPAT) that was then used as an etching mask to form the antidot lattice (ADL) on the graphene (Supplementary information (1)). Atomic force microscopy (AFM) images of ADLG and one antidot formed by optimized low-power Ar gas etching using the NPAT are shown in Fig. 1b. The inset of Fig. 1b proves the hexagonal shape of the antidote (Supplementary information (2) - (4)). Figure 1c shows an STM image obtained in a ~10-layer ADLG with hydrogen termination (Supplementary information (5)). It demonstrates the possible presence of high EDOS (white regions) at the antidot edges on the surface graphene layer, although the high EDOSs are smeared due to the blurred tip of top of the STM probe.

Figure 2a shows a magnetization curve of the hydrogen-terminated monolayer ADLG at T = 2 K (Supplementary information (5)). A ferromagnetic-like hysteresis loop is clearly observed. In contrast, this feature

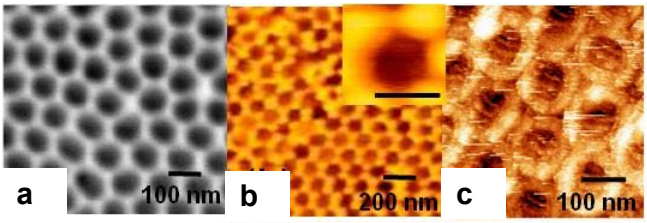

Figure 1. Top view images of samples. a, SEM of a nanoporous alumina template (NPAT) with antidot diameter ϕ ~ 80 nm and antidot spacing L_s ~ 20 nm (i.e., corresponding to the width of GNRs); **b,** AFM of an ADLG formed by using ***a*** as an etching mask; **inset of b,** one antidot in main panel proving its hexagonal shape (the scale bar is 100nm); and **c,** STM of the ~10-layer ADLG obtained at a temperature of 80 K in a constant-current mode. Lighter regions at antidot edges denote higher EDOSs. In the present ADLG, the narrow space between two antidots can be a GNR (Fig.4b). Consequently, the ADLG can provide a large volume of GNRs and edge structures, which result in a large signal of magnetism.

becomes an antimagnetism-like weak hysteresis loop in oxygen-terminated ADLGs (Fig.2b) (Supplementary information (5)). Bulk graphene without antidots show no such features (Fig. 2(c)). These results suggest that ferromagnetism observed in Fig. 2a is strongly associated with the hydrogen-terminated ADL, because this non-lithographic method gives less damage to the antidot edges (Supplementary information (3)) and there are no damage and impurities in bulk graphene regions covered by the NPAT with a thickness over 5 μm. The structure is quite simple and highly reproducible compared with previous graphite-related systems to observe ferromagnetism. To date, 5 samples of the measured 11 samples have shown ferromagnetism like Fig.2a (Supplementary information (5))

Moreover, we find the features observed at T = 2K appear even at room temperature with a larger magnitude of hysteresis loops (Figs. 2d – 2f), although the amplitude of magnetization decreases.

In Fig. 3, magnetizations of the hydrogen-terminated ADL-graphite with the same ADL structure parameters are shown at T = 2K and room temperature. Although ferromagnetic-like hysteresis loops still remain at both temperatures, the magnitude of loops decreases drastically.

The saturation magnetization (M_s) value corresponds to a magnetic moment of ~1.2 $\times 10^2$ μ_B per edge carbon atom (Fig. 2d; μ_B is the Bohr magneton), based on the origin of ferromagnetism discussed later. This value is mostly 100 times larger than those reported in theory[5] and indicates that other carbon atoms possessing weakly localized π-electrons also contribute to magnetization. Assuming that all carbon atoms within 7 nm from the zigzag edge (estimated as ~10^{15}) equally contribute to magnetization, a magnetic moment of ~1.2 μ_B per edge carbon atom is estimated. This value is in good agreement with theory[5].

As mentioned in a latter part, spin interference, caused by

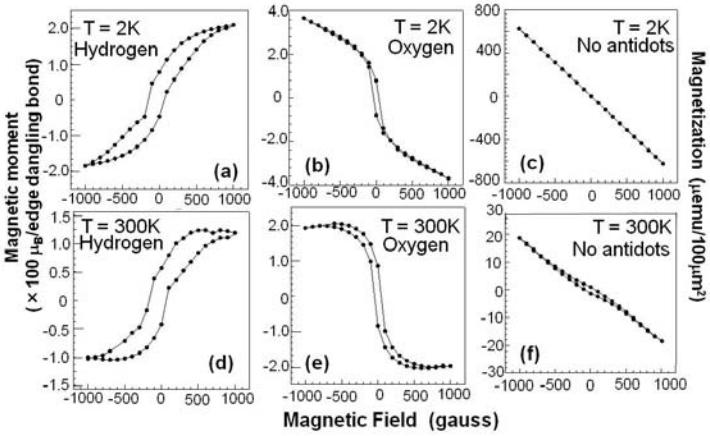

Figure 2. Magnetization of monolayer ADLGs (Supplementary information (5)) with ϕ ~ 80 nm and L_s ~ 20 nm for **a, d** hydrogen-terminated and **b, e** oxygen-terminated antidot edges, and **c, f** bulk graphene without ADL, measured by a superconducting quantum interference device (SQUID; Quantum design) at T= 2K and room temperature, respectively. Magnetic fields were applied perpendicular to the ADLG. Y axis's for a, b, d, and e are noted for magnetic moment per edge carbon atom at dangling bonds of hexagonal antidots, assuming that only the carbon atoms ((estimated as ~10^{13} using two lengths (Fig.4a) and number of carbon atoms of 166/(40 nm length of one boundary of a hexagonal antidot)) have magnetic moment. Those for c and d are just for magnetization per unit area.

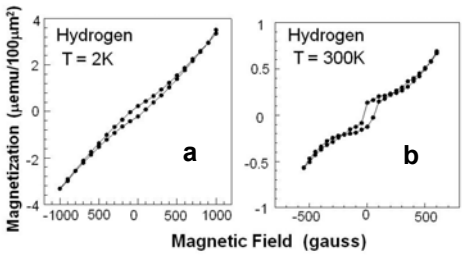

Figure 3. Magnetization of ADL-Graphite with the same ADL structure parameters as those for Fig.2 (with hydrogen-terminated antidot edge), measured at **a** T = 2K and **b** room temperature. Y axis is noted for magnetization per unit area because of unknown layer number and stuck structures of Kish graphite.

both zigzag edges of a GNR, at every carbon site in a GNR determines the appearance of either ferromagnetism or antiferromagnetism (Fig. 4a), depending on termination by foreign atoms and the width of the GNR. The width of space between the present two antidots (i.e., GNR width) of ~20 nm (Fig. 4b) is narrow enough for this spin interference. This implies that carbon atoms located notonly at the zigzag edge but also away from the zigzag edge can actually contribute to magnetization, although carbon atoms located at the dangling bond of the zigzag edge should have magnetic moment larger than ~1.2 μ_B.

The disappearance of the antimagnetism of bulk graphene in ADLGs (Figs. 2c and 2f) is attributed to the formation of ADL, because it drastically reduces the area of bulk graphene sufficient for the presence of loop currents to produce antimagnetism at the presently applied magnetic-field range (i.e., only GNRs with W = ~20 nm

between antidots can correspond to this space (Fig. 4b). The radius of cyclotron motion electrons is given by $R_c = (\pi n_S)^{1/2}(h/2\pi)/eB$. From observing magnetoresistance (i.e., commensurability peak), we estimate $n_S \sim 4 \times 10^{11}$ cm^{-2} in the present ADLGs. Based on this n_s value, R_c is estimated to be as large as ~400 nm even for the presently applied largest magnetic field of 1000 gauss in Fig. 2. Indeed, this R_c value is 20 times larger than W = ~20 nm between the present antidots and prohibits the emergence of loop currents for diamagnetism.

We discuss the origin of the observed ferromagnetism. It is theoretically known that the chemical modification of zigzag-edges GNRs with foreign atoms produces various types of magnetism[3,5-7,9](Supplementary information (6)). In particular, the band structure of mono-hydrogenated and di-hydrogenated GNRs with a large width were shown by tight-binding calculations in Ref. 5 in detail. There are three types for hydrogen terminated edge structures as following. (1) Mono-hydrogenated both edges with a flat band and localized π-orbital edge states at $2\pi/3 \le k \le \pi$. (2) Di-hydrogenated edges on both ends with a flat band and localized edge states at $0 \le k \le 2\pi/3$. (3) Both types of edges present (i.e., GNRs with mono-hydrogenated one side and di-hydrogenated the other side) with a flat band in the whole range of band structures at $0 \le k \le \pi$. Electrons strongly localize at any k values. This case is consistent with Refs. 3 and 4, and the most suitable for the observed ferromagnetism here (Figs.2a and 2d)

The localized electron spins at each edges are ferromagnetically (FM) polarized due to maximizing of exchange energy gain[5]. When the width of a GNR is smaller, two different edge states in different edges for case (3) can be misconceived as an intrinsic property of GNRs. Two different spin configurations are theoretically considered on both edges (Fig. 4a). Under absent hydrogen terminations, antiferromagnetical (AFM) state is stable due to the magnetic tails' interaction which maximizes exchange energy gain (Fig. 4a), while FM state becomes stable when the abovementioned case (2) is realized[5].

From the calculated band structures of the majority and minority spins of the FM configuration and the up- and down-spins of the AFM configuration under case (3)[5], it was found that the FM configuration had a lower energy than the AFM configuration by 4.9 meV per edge atom. Therefore, ferromagnetism can stably emerge in GNRs for case (3). This was also consistent with Ref. 3, which showed that the flat band for up-spins were below E_F and entirely filled, resulting in the appearance of ferromagnetism. The ferromagnetism observed in Figs. 2a and 2d reflects this FM edge configuration.

Here, the regions between the antidots in the present ADLGs behave as GNRs with a width of ~20 nm (Fig. 4b).

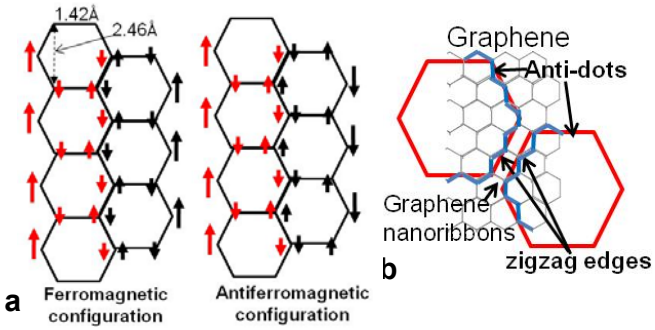

Figure 4. Shematic views of spin configurations of GNRs. **a,** Spin configuration for ferromagnetic and antiferromagnetic ordering in GNRs without hydrogen termination. Arrows mean electron spins on each sites. The dangling bond states localized at the edge contribute significantly to the total magnetic moment with a large exchange splitting, which in turn enhances the exchange splitting of the π-orbital states localized at the edge. Due to the lattice symmetry, the tails of the π-orbital wave function extend into the inner sites of the GNR. The exchange interaction requires the spin ordering on each carbon site to be maximized, similar to Hund's rule for atoms. **b,** Schematic view of graphene masked by an NPAT with hexagonal-shape antidots, showing the alignment of the antidot boundaries with the zigzag edge structure. The space between two antidots corresponds to a GNR with a width of ~20 nm.

Therefore, the ferromagnetism observed in Figs. 2a and 2d correspond qualitatively to case (3). This also suggests presence of zigzag edge at hexagonal antidot edges (Supplementary information (7)). This is consistent with STM observation (Fig.1c).

On the other hand, Ref. 6 reported that the formation of a spin-paired carbon-oxide (C–O) bond drastically reduced the local atomic magnetic moment of carbon at the zigzag edge of GNRs and suppressed the emergence of ferromagnetism. The disappearance of ferromagnetism in Figs. 2b and 2e can be qualitatively consistent with this configuration.

Moreover, Ref. 7 showed that regardless of the stacking sequences, either AB or AA, the magnetic moment caused by the localized orbital states disappears upon the interlayer stacking of graphite with hydrogen-terminated edges. This also qualitatively explains the reduced ferromagnetic-like loops in Fig. 3.

Although an atomic-scale observation of the edge structures (Supplementary information (7)) is indispensable to confirm this discussion, all the present results are qualitatively consistent with theories. Apart from the edge effect, Ref. 13 also predicted the appearance of ferromagnetism in ADLGs with honeycomb-shaped antidots from a group-theoretical consideration based on the tight-binding model. Although the study did not mention edge termination by foreign atoms, the structures directly correspond to the present ADLGs with honeycomb-shaped antidots (Fig. 1b) and might explain the present ferromagnetism.

Here, three reasons are considered about why evident

ferromagnetism can be observed in the present system as following. Approximately 50% of the fabricated hydrogen -annealed ADLG samples (number of 5/11; Supplementary information (5)) have exhibited ferromagnetism to date.

(1) The benefit of the non-lithographic fabrication method, which exploits NPAT in conjunction with low-power gas etching and high-temperature annealing. This process ensures only slight damage to the graphene edges. (2) The lattices of the hexagonal-shaped antidots can result in the formation of a large number of GNRs with sufficient length (e.g., 40 nm in the present case) due to the presence of six boundaries among the neighbouring six antidots for each one antidot in comparison with lattices of the square- and round-shaped antidots. In the actual ADLG, it is speculated that zigzag- and arm-chair edges exist with mixed states in one GNR (one boundary), as in the STM observation in Ref. 9. Nevertheless, the large number of GNRs in the present ADLGs can yield a large area of assembled zigzag-edge GNRs. (3) The hexagonal-shaped antidot transferred from the pore of the NPAT. When a hexagonal-shaped antidot is fabricated on graphene consisting of hexagonal carbon lattices, the six boundaries (edges) of an antidot tend to have the same atomic structure (Fig. 4b). Once an NPAT mask is placed onto the graphene so that one boundary of the antidot coincides with the zigzag edge, all the antidot edges acquire a zigzag structure.

These three factors have an equal probability for antidots with a zigzag, arm-chair, or mixed structure (Supplementary information (7)). However, if only the zigzag edge is likely to be formed with low damage by Ar gas etching as it is the most stable, these advantages will effectively contribute to the observed ferromagnetism.

Recently, the possibility of a spin filtering effect[22] and a (quantum) spin Hall effect (QSHE)[25-27] utilizing edge spin current of graphene has been predicted, assuming enhanced spin-orbit interaction. SHE is expected to realize novel spintronic devices[24], because electron spins are controlled by electric fields and are carried without energy dissipation even in paramagnetic materials. The ferromagnetism observed here turned out spin polarization at the graphene zigzag edge and promises the appearance of a large-magnitude spin current. This must open a new door to a 2-D (Q)SHE and carbon spintronic devices by modulating flat bands.

1. Nakada, K., Fujita, M., Dresselhaus, G. and Dresselhaus, M. S., Edge state in graphene ribbons: nanometer size effect and edge shape dependence. *Phys. Rev. B* **54**, 17954–17961 (1996).
2. Fujita, M. et al. Peculiar localized state at zigzag graphite edge. *J. Phys. Soc. Jpn.* **65**, 1920–1923 (1996).
3. Kusakabe, K. and Maruyama, M., Magnetic nanographite. *Phys. Rev. B* **67**, 092406 (2003).
4. Okada, S. and Oshiyama, A., Magnetic Ordering in Hexagonally Bonded Sheets with First-Row Elements. *Phys. Rev. Lett.* **87**, 146803 (2001).
5. Lee, H. et al., Magnetic ordering at the edges of graphitic fragments: Magnetic tail interactions between the edge-localized states. *Phys. Rev. B* **72**, 174431 (2005)
6. Veiga, R. G. A. et al., Quenching of local magnetic moment in oxygen adsorbed graphene nanoribbons. *J. Chem. Phys.* **128**, 201101 (2008).
7. Lee, H. et al., Ferromagnetism at the edges of the stacked graphitic fragments: an ab initio study. *Chem. Phys. Lett.* **398** 207–211 (2004).
8. Cervenka, J. et al., Room-temperature ferromagnetism in graphite driven by two-dimensional networks of point defects. *Nature Phys.* **5**, 840–844 (2009).
9. Enoki, T. et al., The edge state of nanographene and the magnetism of the edge-state spins. *Sol. Stat. Comm*. **149**, 1144–1150 (2009).
10. Niimi, Y. et al., Scanning tunneling microscopy and spectroscopy of the electronic local density of states of graphite surface near monoatomic step edges. *Phys. Rev. B* **73**, 085421 (2006).
11. Son, Y-W., Cohen, M. L. and Louie, S. G., Energy gaps in graphene nanoribbons. *Phys. Rev. Lett*. **97**, 216803 (2006).
12. Yang, L. Louie, S. G., et al., Quasiparticle energies and band gaps in graphene nanoribbons *Phys. Rev. Lett.* **99**, 186801 (2007).
13. Shima, N. and Aoki. H., Electronic structure of superhoneycomb systems. *Phys. Rev. Lett*. **71**, 4389–4392 (1993).
14. Rosser, J. F. and Palacios, J. J., Magnetism in graphene nanoislands. *Phys. Rev. Lett*. **99**, 177204 (2007).
15. Jia, X. M. et al., Controlled formation of sharp zigzag and armchair edges in graphitic nanoribbons. *Science* **323**, 1701–1705 (2009).
16. Girit, C. O. et al., Graphene at the edge: stability and dynamics. *Science* **323**, 1705–1708 (2009).
17. Shimizu, T., Haruyama, J., et al., Large intrinsic energy bandgaps in annealed nanotube-derived graphene nanoribbons. *Nature Nanotech*. Advance online publication (19th December 2010).
18. Han, M. Y., et al., Electron transport in disordered graphene nanoribbons. *Phys. Rev. Lett*. **104**, 056801 (2010).
19. Wang, X., et al., Room-temperature all-semiconducting sub-10-nm graphene nanoribbon field-effect transistors. *Phys. Rev. Lett.* **100**, 206803 (2008).
20. Bai,J., Zhong, X. et al., Graphene nanomesh. *Nature Nanotech*. **5**, 190-194 (2010).
21. Russo, S., et al., Observation of Aharonov-Bohm conductance oscillations in a graphene ring. *Phys. Rev. B* **77**, 085413 (2008).
22. Son, Y-W., Cohen, M. L. and Louie, S. G., Half-metallic graphene nanoribbons. *Nature* **444**, 347–349 (2006).
23. Takesue, I., et al., Superconductivity in entirely end-bonded

multiwalled carbon nanotubes. *Phys. Rev. Lett.* **96**, 057001 (2006).

24. Murakami, S., Nagaosa, N., and Zhang, S. C., Dissipationless quantum spin current at room temperature. *Science* **301**, 1348–1351 (2003).
25. Kane, C. L. and Mele, E. J., Quantum spin Hall effect in graphene. *Phys. Rev. Lett*. **95**, 226801 (2005).
26. Kane, C. L., Graphene and quantum spin Hall effect. *J. Modern Phys. B* 21, 1155–1164 (2007).
27. Schmidt, M. J. and Loss, D., Edge states and enhanced spin-orbit interaction at graphene/graphane interfaces. *Phys. Rev. B* **81**, 165439 (2010).

Acknowledgements

The authors wish to thank S. Tarucha, M. Yamamoto, H. Aoki, N. Nagaosa, A. Oshiyama, K. Fujita, Y. Hashimoto, E. Endo, Y. Iye, S. Katsumoto, T. Ando, M. Koshino, T. Enoki, J. Akimitsu, T. Muranaka, K. Nakada, P. Kim, and M. S. Dresselhaus for their technical contribution, fruitful discussions, and encouragement. The work at Aoyama Gakuin was partly supported by a Grant-in-aid for Scientific Research and a High-Technology Research Center Project for private universities in MEXT.

Author contributions

J.H. conceived and designed the experiments. K.T., S.K., and Y.Y. performed the experiments. J.H. analyzed the data and wrote the paper. T.M. and H.F. contributed to the STM observations.

Additional information

Correspondence and requests for materials should be addressed to J.H. (J-haru@ee.aoyama.ac.jp).